J Therm Anal Calorim (2013) 113:319–328
DOI 10.1007/s10973-012-2844-y

Crystal structure, electronic structure, and bonding properties of anhydrous nickel oxalate

Andrzej Koleżyński · Bartosz Handke · Ewa Drożdż-Cieśla

Received: 15 October 2012 / Accepted: 21 November 2012 / Published online: 23 December 2012

Abstract The results of crystal structure determination and theoretical analysis of electronic structure and bonding properties in relation to thermal decomposition process in anhydrous nickel oxalate are presented. The details of the methods used in this analysis i.e., the Bader's quantum theory of atoms in molecules and bond order models (as defined by Pauling, Bader, Cioslowski and Mixon—modified by Howard and Lamarche), applied to topological properties of the electron density, obtained from ab initio calculations carried out by Wien2k FP-LAPW package (full potential linearized augmented plane wave method), as well as Brown's bond valence model (bond valences and strengths, and bond and crystal strains, calculated from experimental crystal structure data) are described. Nickel oxalate dihydrate was prepared by precipitation from water solutions of nickel nitrate (V) with oxalic acid at about 60 °C. The crystalline powder was filtered, washed, and dried at 80 °C on air. Anhydrous nickel oxalate sample was measured by XRD method applying Philips X'Pert Pro MD diffractometer equipped with MRI high temperature cell. Structural as well as qualitative and quantitative phase analyses were made by Phillips X'Pert HighScore Plus version 2.1 software with implemented full-pattern fit by means of Rietveld method. The detailed analysis of the obtained results shows that anhydrous nickel oxalate has monoclinic crystal structure ($P2_1/c$, sg 14), the carbon–carbon bond is the weakest one, and the process of thermal decomposition of this structure should begin with the breaking of this particular bond followed by nickel-oxygen bonds, which will lead to metallic nickel and carbon dioxide as final products, in agreement with the experiment. These results, supported by our earlier ones show clearly that such methods (topological and structural), when used simultaneously in analysis of the crystal structure and bonding properties, provide us with the additional insight into the behavior of given compound during thermal decomposition process and thus allow predicting and explaining of its most probable pathway.

Keywords Crystal structure bond order · Bond strength · Bond valence · Electron density topology · FP-LAPW DFT calculations · Thermal decomposition of anhydrous nickel oxalates

A. Koleżyński (✉) · B. Handke · E. Drożdż-Cieśla
Faculty of Materials Science and Ceramics, AGH University of Science and Technology, Al. Mickiewicza 30, 30-059 Krakow, Poland
e-mail: andrzej.kolezynski@agh.edu.pl

Introduction

Anhydrous nickel oxalate belongs to the isostructural family of anhydrous metal oxalates β-MeC_2O_4 (where Me is Fe, Co, Ni, Zn, Cu—Kondrashev et al. [1]; Cd—Jeanneau et al. [2]), with monoclinic unit cell $P2_1/n$, with similar cell parameters, arrangement of the MeO_6 octahedra and oxalate anions, but different thermal decomposition to Me, MeO, or $MeCO_3$ [3–11]. In a series of previously carried out calculations [12–18] we have applied theoretical approach based on ab initio DFT FP-LAPW calculations in order to describe the bonding properties of different anhydrous oxalates and their relation to thermal decomposition pathway, characteristic for a given compound. Since there is no detailed crystallographic data for anhydrous nickel oxalate crystal structure available (at least we were unable to find it) in order to carry out ab initio calculations of electronic structure and topological properties of total electron density allowing us to analyze

electronic structure and bonding properties and providing us with additional insight into the thermal decomposition process and necessary means to explain thermal decomposition pathway in anhydrous nickel oxalate, we decided to synthesize nickel oxalate hydrate and conduct a series of XRD measurements for different temperatures to obtain necessary data.

In this paper we present the results of the synthesis, structural analysis, and theoretical studies undertaken for anhydrous nickel oxalate. The obtained results of XRD structural analysis, ab initio electronic structure calculations, bond orders, and bond valences are discussed in the light of the thermal decomposition process.

Synthesis and XRD analysis

Nickel oxalate dihydrate was prepared by precipitation from water 0.05 M solutions of oxalic acid and nickel nitrate. During precipitation, solution was stirred vigorously. pH mixture 4.0 ± 0.1 was mentioned with ammonia and hydrochloric acid to avoid precipitation of nickel hydroxide. The mixture was kept at about 60 °C for 4 h in order to salt powder aging. The crystalline powder was filtered, washed with dilute oxalic acid and next with an absolute alcohol, and finally dried at 80 °C on air. All used reagents were of analytical grade Polskie Odczynniki Chemiczne S.A.

The obtained samples were used in XRD measurements applying Philips X'Pert Pro MD diffractometer equipped with MRI high temperature cell. Standard Bragg–Brentano geometry was applied with $K\alpha_1$ monochromatic beam from Cu anode. All measurements were performed in air with the 0.008 ° step size in the 15–60 ° scanning range and the 48 s of measurement time for each step. Powder sample was placed directly on the platinum strip heater; therefore, reflections from Pt around 40 and 46.5 ° are present in the collected data. The platinum strip was resistively heated at the speed of 15 K min^{-1} and the desired temperature was stabilized for 15 min before each measurements. Temperature was measured by Pt–Ir thermocouple spot welded to the other side of the heater. The PID controller was used in order to avoid overshooting of the desired temperature thus excluding hysteresis effect. Structural as well as qualitative and quantitative phase analyses were made by Phillips X'Pert HighScore Plus version 2.1 software with implemented full-pattern fit by means of Rietveld method.

In the Fig. 1 the contour plot for series of XRD measurements vs temperature are presented. The reflections intensity are represented by shades of gray. Clear history of $NiC_2O_4{\cdot}H_2O$ decomposition into NiC_2O_4 and finally into NiO is visible. Peaks around 40 an 46.5 ° visible as a straight lines are artifacts from Pt heater. Along

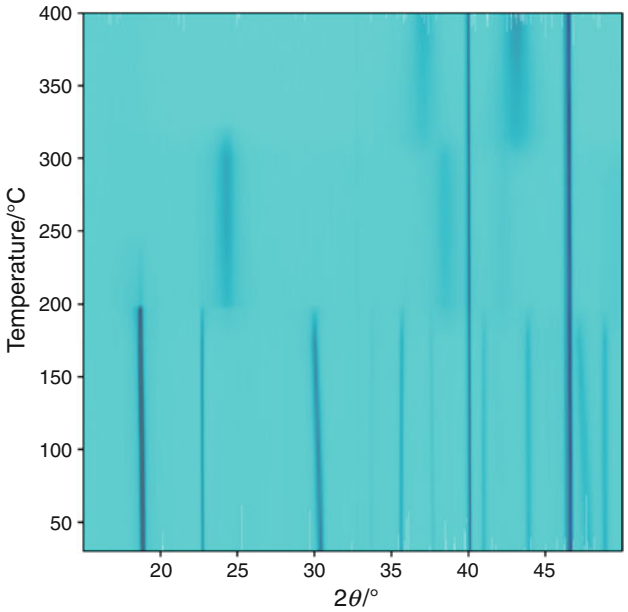

Fig. 1 Contour *plot* for XRD measurements versus temperature

temperature axis, there are two distinct changes in number and reflection position. The first change, close to 200 °C takes place when *C*2/*c* phase of hydrated oxalate changes into $P2_1/c$ phase of pure oxalate. Second transition, is the decomposition of oxalate into cubic form NiO around 300 °C. It is worth to note the fact of coexistence of phases at relatively wide temperature regions of about 20–50 °C (it would not be surprising in fast measurements, but in case of XRD the single scan took over 50 min including the time needed for temperature stabilization).

The XRD data collected at three temperatures: 30, 300, and 365 °C, for three distinct phases, are shown in Fig. 2. Black solid line represents full-pattern fit for each phase. There are no crystallographic data for $NiC_2O_4{\cdot}H_2O$ as well as for NiC_2O_4 in the literature, in order to perform full-pattern fit. Nevertheless, we have found structural similarities with other, cobalt oxalate—CoC_2O_4. On a basis of the structural model for $CoC_2O_4{\cdot}H_2O$ and CoC_2O_4, the Co ion was substituted with Ni ion. That gave reasonable fitting result with structural details gathered in Table 1. Broad peaks for NiC_2O_4 as well as for NiO imply small crystallite sizes around 100 nm. Diffraction patterns also exhibit effects from preferred (111) orientation of the crystallites.

Crystal structure

The crystal structure of anhydrous nickel oxalate is very similar to the structures of anhydrous zinc and cobalt oxalates [14, 15] and can be described as built from $–C_2O_4–Ni–C_2O_4–Ni–$ chains, or alternatively as layered

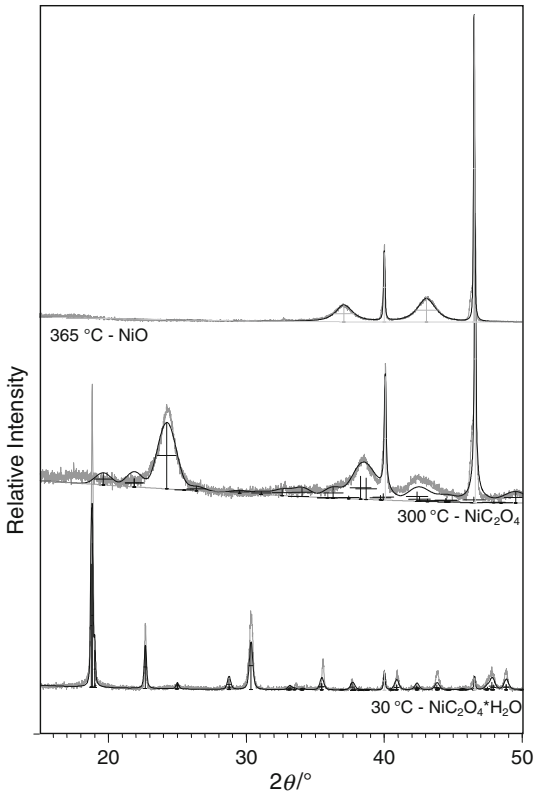

Fig. 2 Diffraction pattern for chosen temperatures: 30, 250, and 365 °C, corresponding to $NiC_2O_4{\cdot}H_2O$, NiC_2O_4, and NiO phase, respectively. The intensity scale for each pattern is not normalized to each other in order to emphasize the details

material, formed by cationic layers built from corner-shared NiO_6 octahedra, linked together via bidentate chelating oxalate groups (Fig. 3).

Each nickel atom is surrounded by six oxygen atoms, all belonging to oxalate groups: two O_1 and four O_2 atoms, forming highly elongated octahedron (the lengths of Ni–O bonds are 2.301, 2.321, and 2.604 Å; NiO_6 octahedron volume is equal to 16.34 $Å^3$ and respective angles between Ni and O bonds in octahedron are 68.31, 72.60, and 89.21 °). In each nickel octahedron, all four O_2 atoms are shared by two octahedra belonging to neighboring chains, almost perpendicular to each other. Similarly as in case of anhydrous cobalt and zinc oxalates, one can analyze the crystal structure of $Ni_2C_2O_4$ from a point of view of local environment of a given octahedron or oxalate anion: every octahedron is surrounded by four oxalate anions (Fig. 4a), each of which is in turn surrounded by four NiO_6 octahedra (Fig. 4b). In Fig. 4c the oxalate anion with bonds labeled are shown, while in Table 1 the results of crystal structure parameters and in Table 2 fractional coordinates and respective Wyckoff's positions obtained from XRD measurement for anhydrous nickel oxalate are presented.

Computational details

The ab initio calculations of electronic structure and topological properties of total electron density in NiC_2O_4 crystal have been carried out by means of WIEN2k FP-LAPW ab initio package [19] within density functional theory (DFT) formalism [20–25]. The following parameters has been chosen for the calculations: 500 *k*-points ($9 \times 7 \times 6$ mesh within the irreducible Brillouin zone), cut-off parameter $Rk_{max} = 7.5$ and GGA–PBE exchange–correlation potential [26]; the values of muffin-tin radii (R_{MT}) (a.u.): Ni–1.8, O–1.17, C–1.17 and the convergence

Table 1 Structural parameters for calculated full-pattern fit of XRD measurements

Chemical formula	Space group	Unit cell parameters					
		a/Å	b/Å	c/Å	α/°	β/°	γ/°
$NiC_2O_4{\cdot}H_2O$	*C*2/*c*	11.716(2)	5.3217(9)	9.718(2)	90	126.790(8)	90
NiC_2O_4	$P2_1/c$	5.217(9)	5.477(4)	6.921(4)	90	118.65(7)	90
NiO	*Fm*3*m*	8.405(1)	8.405(1)	8.405(1)	90	90	90

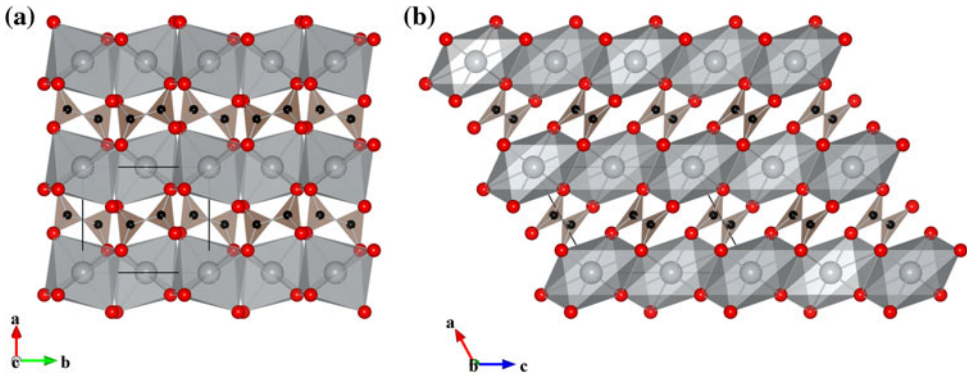

Fig. 3 Crystal structure of anhydrous nickel oxalate

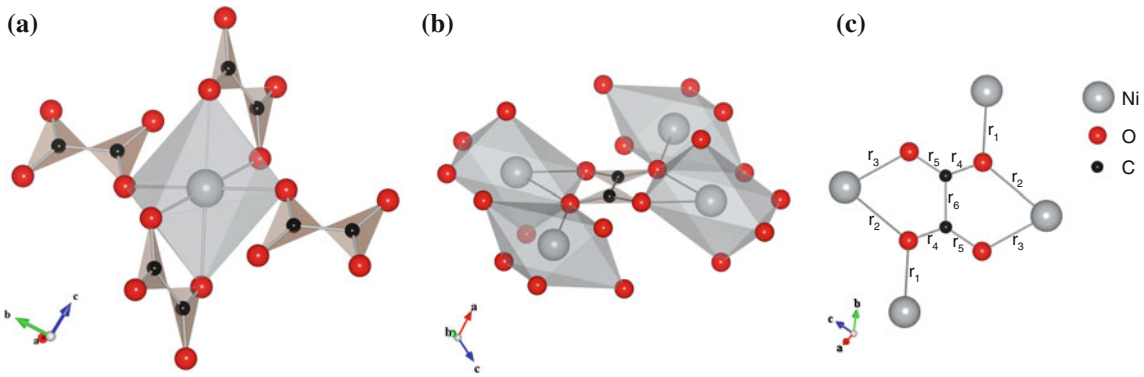

Fig. 4 Local environments of NiO_6 octahedron (**a**) and oxalate anion (**b**) and the same anion but with bonds labels depicted (**c**)

Table 2 Atomic fractional coordinates in anhydrous nickel oxalate obtained from XRD measurements

Space group		$P2_1/c$ (no. 14)		
Atom	x	y	z	Wyckoff's positions
Ni	0	0	0	2a
O_1	0.2110	0.1954	0.3896	4e
O_2	0.3732	0.7695	0.2625	4e
C	0.5451	0.8782	0.4619	4e

criteria for SCF calculations: $\Delta E_{SCF} \leq 10^{-5}$ Ry and $\Delta\rho_{SCF} \leq 10^{-5}$ e for total energy and electron density, respectively. The calculations were carried out with and without spin polarization in order to check the influence of spin polarization on topological properties of bond critical points. The band structure was calculated for selected path along high symmetry points defined for monoclinic unit cell (SG no. 14 on Bilbao Crystallographic Server [27–29]).

The obtained total SCF electron density distribution in crystal cell served as a basis for the calculations of topological properties of bond critical points (within Bader's quantum theory of atoms in molecules [30] formalism). These results have been used in calculations of bond orders as defined by Pauling [31], Bader [32], Cioslowski and Mixon [33] (modified by Howard and Lamarche [34]) and bond valences, according to the Bond Valence Method (an excellent review of BVM can be found in Brown [35]). The more detailed description of methods used in present calculations can be found in our previous papers [12, 13].

Results

Electronic structure

Since nickel belongs to transition metals with partially filled *d*-subshell (electron configuration $[Ar]3d^8 4s^2$), for electronic structure calculations spin polarization had to be taken into account (the calculations carried out for the case without spin polarization suggested wrongly the metallic properties of anhydrous nickel oxalate). The spin polarized band structure calculated for selected path along high symmetry points with respective densities of states projected onto particular atoms is presented in Figs. 5 and 6 (for spin-up and spin-down electron density, respectively).

Apart from obvious differences between band structures calculated for opposite spin electron densities, there are clear similarities (also with the respective band structures obtained for different *d*-electron metals anhydrous oxalates presented in our earlier papers [12–15, 17, 36]) nickel 3*d* electrons populate mostly valence bands close to Fermi energy. Despite the fact that as in the case of zinc [14] the lack of deeper lying *d* sub-shells with the same symmetry results in not so effective screening of 3*d* electrons as in case of silver or cadmium [12, 36], due to spin polarization resulting in effective "pushing out" of minority spin-down electrons toward the higher energies (Figs. 5, 6) and in the same time higher energy dispersion comparing to majority spin-up electrons, the resulting nickel 3*d* atomic orbitals are more diffuse than those in zinc and their size look like respective ones in cadmium. As a result, the respective metal–oxygen bonds are longer in anhydrous nickel oxalate than in anhydrous zinc oxalate (these lengths, when no other effects e.g., geometrical ones are present, depends practically entirely on minimization of the energy due to the maximization of respective overlap integrals calculated for electron density localized in the region between respective atoms i.e., on the degree of metal 3*d* and oxygen 2*p* orbitals overlapping).

More detailed analysis of band structure and densities of states projected onto particular atomic orbitals (Fig. 7) shows that nickel majority (spin up) 3*d* electrons (Fig. 7a) fill mostly narrow bands with energies from −4 eV up to Fermi energy, while minority electrons fill valence bands lying close to Fermi energy and few others lying in the

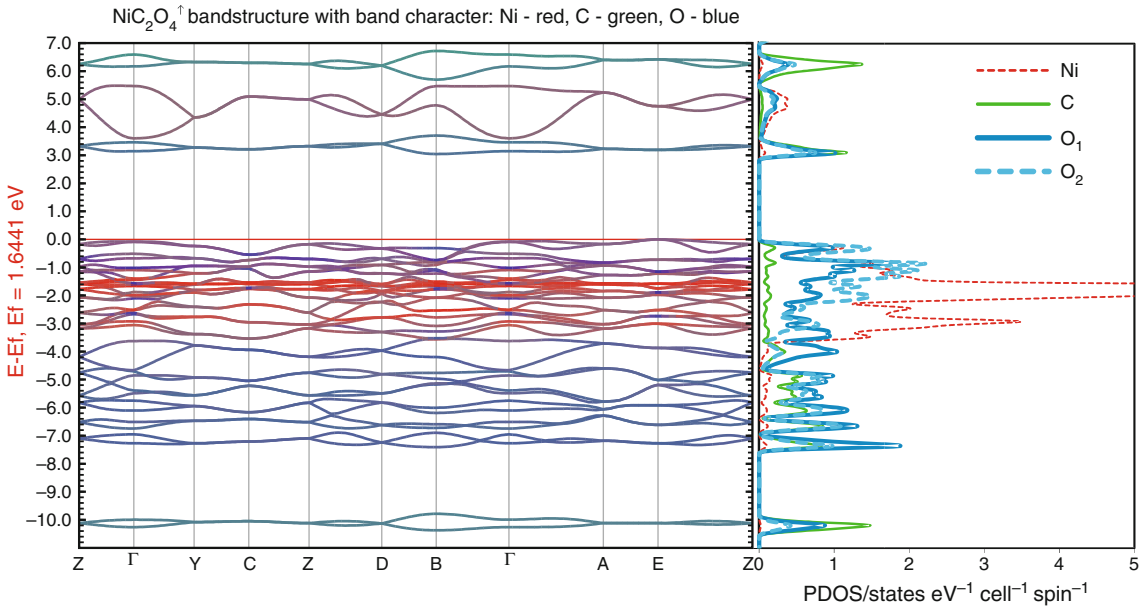

Fig. 5 Band structure with band character represented by mixture of RGB colors (assigned to Ni, C, and O character, respectively; *in color on-line*) and partial densities of states (projected onto particular atoms) obtained for anhydrous nickel oxalate by means of DFT FP-LAPW calculations for majority electrons (spin-up electron density)

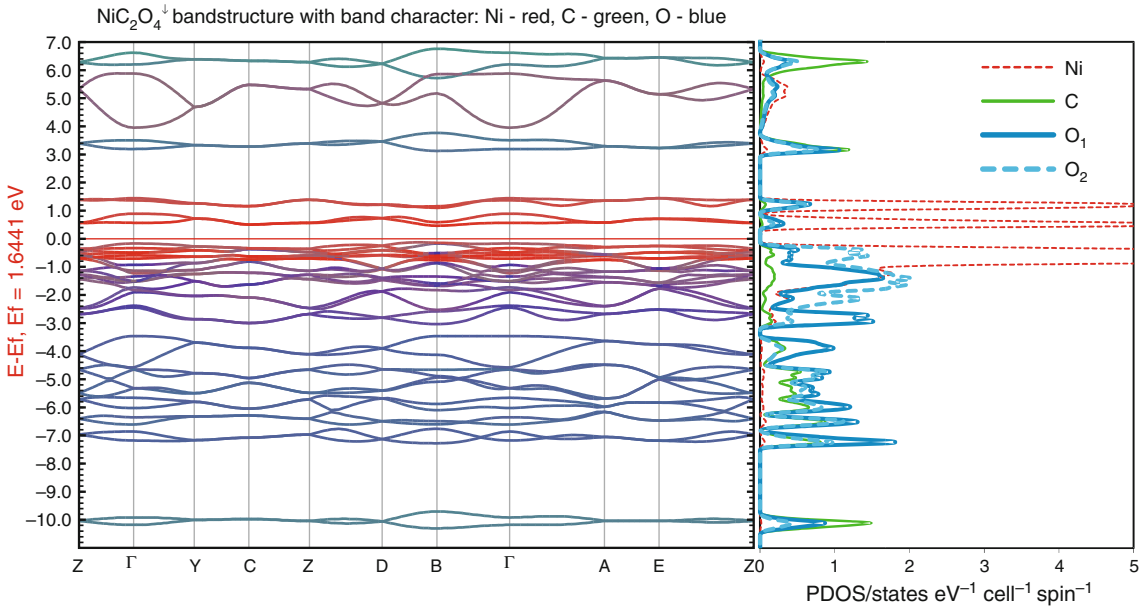

Fig. 6 Band structure with band character represented by mixture of RGB colors (assigned to Ni, C, and O character, respectively; *in color on-line*) and partial densities of states (projected onto particular atoms) obtained for anhydrous nickel oxalate by means of DFT FP-LAPW calculations for minority electrons (spin-down electron density)

energy range corresponding to energy gap in case of electronic structure for majority electrons. Nickel 4*s* electrons (when in excited state) fill mainly bands in conduction band at energies about 5 eV. In case of carbon and oxygen atoms the effects due to spin polarization are negligible (Fig. 7b, c, d). Partial densities of states obtained for oxygen atoms O_1 and O_2 show, similarly as in anhydrous zinc oxalate, different patterns of states occupation—2*p* electrons in O_1 oxygen atom fill quite uniformly bands with the energies between −7 eV and Fermi energy and too much lower extent very narrow, deeper lying bands with energies about −18 i −21 eV and also (when in excited state) to some extent bands lying conduction band. In case of O_2 oxygen atom, 2*p* electrons,

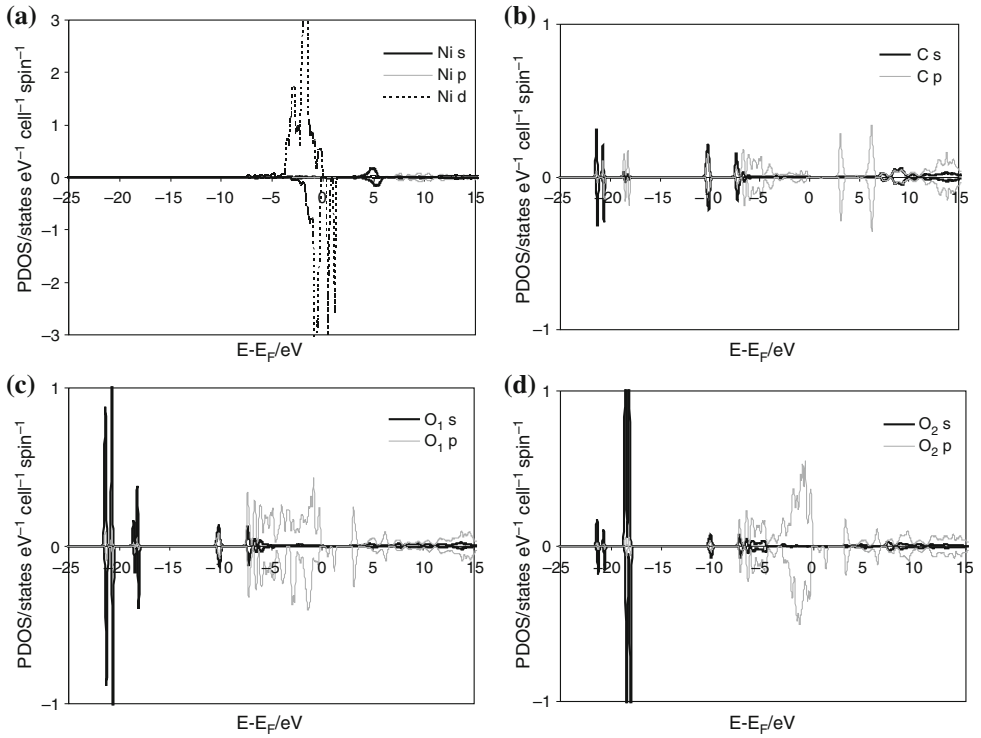

Fig. 7 Densities of states projected onto particular atomic orbitals, obtained for anhydrous nickel oxalate by means of DFT FP-LAPW calculations (positive and negative values correspond to spin-up and spin-down electron density, respectively)

besides similarities to 2*p* electrons in O_1 oxygen atom for bands with the energies −18 i −21 eV and conduction bands, also indicate essential difference, namely the distinct asymmetry in band occupation for bands lying close to Fermi energy (much higher share in bands occupation in energy range between −3 eV and Fermi energy and relatively small one in occupation of bands with energy in a range −7 to −3 eV). 2*s* electron of O_1 oxygen atoms fill mostly well localized bands with the energy about −21 eV and also, too much smaller extent, bands with energy −18 and −10 eV and bands in energy range from −7 to −5 eV, whereas 2*s* electrons of O_2 oxygen atoms dominate in bands with the energy −18 eV and to smaller extent bands with energy −21 eV, and also—like 2*s* electrons of O_1 atoms—bands with the energy about −10 eV and within energy range from −7 to −5 eV. Carbon 2*s* electrons fill the same narrow bands as oxygen electrons (−21, −18, −10, −7 eV), and 2*p* electrons, besides the same narrow bands as 2*s* electrons, fill additionally bands close to Fermi energy (−7, 0 eV).

From the results presented above, the following picture of bonding in anhydrous nickel oxalate emerges: weak nickel—oxygen bonds are formed as a result of the interactions between nickel 3*d* and oxygen 2*p* electrons. Carbon 2*s* and one 2*p* electrons fill hybridized carbon orbitals (sp^2 hybridization) and form 3 σ bonds with two oxygen atoms and second carbon atom within oxalate anion, while the second carbon 2*p* electron forms conjugated π* bond with two neighboring oxygen atoms.

Electron density topology

The results of topological analysis of total non spin polarized and spin polarized electron density in anhydrous nickel oxalate (obtained from DFT FP-LAPW calculations), carried out according to Bader's QTAiM formalism are presented in Tables 3 and 4, respectively. QTAiM total charges calculated by means of CRITIC [37] program for nickel, carbon, and oxygen O_1 and O_2 pseudoatoms are equal to +1.070, +1.062, −0.769, and −0.828, respectively.

Detailed analysis of the obtained results show that despite the necessity of taking spins into account in DFT FP-LAPW calculations, all bonds can be divided into three distinct groups (identically as in case of other anhydrous *d*-electron metal oxalates, analyzed earlier): (a) metal–oxygen bonds (small value of electron density at bond critical point $\rho_{BCP}(r)$, positive value of electron density Laplacian $\nabla^2\rho(r)$—properties characteristic for closed shell interactions, weak ionic-covalent bonds with strong ionic character), (b) carbon–oxygen bonds (large values of electron density at BCP and strongly negative values of

Table 3 Bond critical points (BCP) properties in anhydrous nickel oxalate crystal calculated for DFT FP-LAPW total non spin polarized electron density: bond length R, Hessian matrix eigenvalues λ_1–λ_3, electron density $\rho_{BCP}(r)$, Laplacian $\nabla^2\rho(r)$, ellipticity, electrostatic potential $V(R)$, electronic $H_e[\rho(r)]$ and kinetic $G[\rho(r)]$ energies and bond orders (Cioslowski and Mixon formula [33], modified by Howard and Lamarche [34])

NiC_2O_4	R/Å	λ_1/e·Å^{-5}	λ_2/e·Å^{-5}	λ_3/e·Å^{-5}	$\rho_{BCP}(r)$/e·Å^{-3}	$\nabla^2\rho(r)$/e·Å^{-5}	ε	V[$\rho(r)$]/au	$H_e[\rho(r)]$/au	G[$\rho(r)$]/au	$n_{CM(HL)}$
r_1 (Ni–O_1)	2.323	−0.958	−0.932	5.070	0.265	3.181	0.027	−0.393	−0.177	0.216	0.83
r_2 (Ni–O_1)	2.608	−0.449	−0.435	2.415	0.143	1.531	0.032	−0.623	−0.302	0.321	0.80
r_3 (Ni–O_2)	2.301	−1.008	−0.969	5.324	0.279	3.347	0.040	−0.609	−0.291	0.318	0.83
r_4 (C–O_1)	1.257	−23.032	−22.969	31.932	2.585	−14.079	0.003	−1.698	−0.922	0.776	1.13
r_5 (C–O_2)	1.371	−15.949	−13.819	9.980	2.068	−19.788	0.154	−1.180	−0.692	0.487	0.89
r_6 (C–C)	1.590	−11.078	−10.102	9.676	1.525	−11.505	0.097	−2.013	−1.103	0.910	0.71

Table 4 Bond critical points (BCP) properties in anhydrous nickel oxalate crystal calculated for DFT FP-LAPW total spin polarized electron density: electron density $\rho^{\uparrow\leftarrow\leftarrow}(r)$ and $\rho^{\downarrow}(r)$, Laplacian $\nabla^{2\leftarrow}\rho^{\leftarrow\uparrow}(r)$ and $\nabla^2\rho^{\downarrow}(r)$, electrostatic potential $V[\rho^{\uparrow}(r)]$ and $V[\rho^{\downarrow}(r)]$, and electronic energy $H_e[\rho^{\uparrow}(r)]$ and $H_e[\rho^{\downarrow}(r)]$

NiC_2O_4	$\rho^{\uparrow\leftarrow\leftarrow}(r)$/e·au^{-3}	$\rho^{\downarrow}(r)$/e·au^{-3}	$\nabla^{2\leftarrow}\rho^{\leftarrow\uparrow}(r)$/e·au^{-5}	$\nabla^2\rho^{\downarrow}(r)$/e·au^{-5}	$V[\rho^{\uparrow}(r)]$/au	$V[\rho^{\downarrow}(r)]$/au	$H_e[\rho^{\uparrow}(r)]$/au	$H_e[\rho^{\downarrow}(r)]$/au
r_2 (Ni–O_1)	0.017	0.016	0.110	0.046	−0.628	−0.600	−0.300	−0.294
r_1 (Ni–O_1)	0.013	0.009	0.070	0.009	−0.340	−0.235	−0.161	−0.116
r_3 (Ni–O_2)	0.019	0.018	0.077	0.031	−0.568	−0.567	−0.274	−0.280
r_4 (C–O_1)	0.191	0.191	−0.293	−0.293	−1.694	−1.694	−0.884	−0.883
r_5 (C–O_2)	0.153	0.153	−0.407	−0.414	−1.173	−1.174	−0.637	−0.639
r_6 (C–C)	0.121	0.119	−0.393	−0.377	−1.718	−1.707	−0.908	−0.901

Laplacian–interactions with shared density, localized in bonding region; polar bonds with dominating covalent character), and (c) carbon–carbon bonds (relatively large values of electron density at BCP and strongly negative values of Laplacian—interactions with shared density, localized in bonding region; characteristic for oxalates covalent bonds, weaker than carbon–oxygen bonds).

It follows from the results presented in Tables 3 and 4 that strong asymmetry of the NiO_6 octahedra do not influence in distinct way the character and properties of bond critical points, which despite the similarities to the properties of BCPs in anhydrous zinc oxalate [14] (clear asymmetry of the properties of carbon–oxygen bonds, but not so significant as in ZnC_2O_4 and almost no such asymmetry in case of metal–oxygen bonds) are much more like the respective BCPs in anhydrous cadmium oxalate [13]. One can see that C–C bond (r_6) in anhydrous nickel oxalate is the weakest one, Ni–O bonds are stronger than C–C bonds, but weaker than C–O bonds (r_5 bond is only slightly stronger than Ni–O bonds, but due to the much deeper potential well in the proximity of BCP for this bond in comparison with Ni–O bonds and thus more negative total electronic energy, this bond should be energetically more durable than r_1–r_3 bonds).

The data collected in Table 4 show also that the properties of the electron density at bond critical points are significantly independent on spin polarization. This conclusion has been confirmed by the calculations we have carried out for non spin polarized density and comparison of the properties of BCPs for total non spin polarized density and total spin density. The calculations showed that respective BCP properties are almost identical, especially in a case of BCPs calculated for C–O and C–C bonds. In the case of Ni–O bonds, the differences concern mostly the positions of BCPs and values of the parameters characterizing their properties, but do not change at all the overall picture of the topological properties of this compound. The lack of significant quantitative and qualitative differences between the topological parameters of electron densities obtained in calculation with and without spin polarization stems from the fact that changes in total electron density distribution due to spin polarization are more significant mostly close to nickel atoms while being much less important for the rest of the atoms (Fig. 8), and in the proximity of BCPs these differences are practically negligible. The polarization of 3*d* electrons, due to their odd number causes weaker screening of majority electrons, thus they feel stronger effective core potential and are concentrated closer to nickel cores, while minority electrons, being better screened are more diffused (Fig. 9) and this is a reason why mostly these electrons take part in bond formation with oxygen atoms, forcing loosening of the

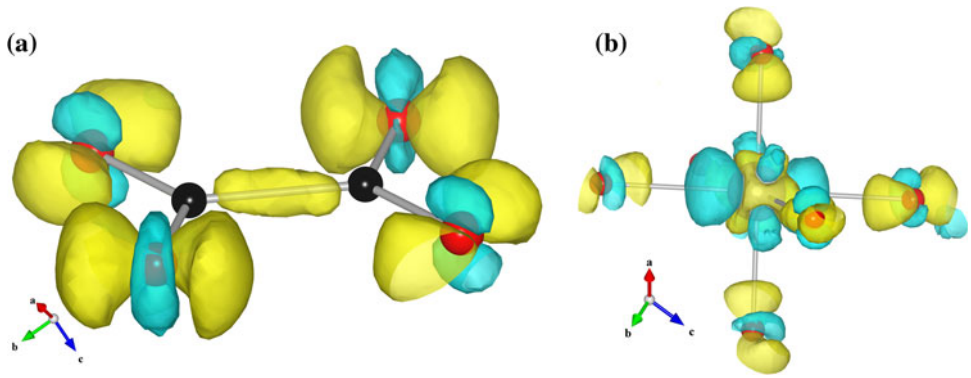

Fig. 8 Differential map of total electron density in anhydrous nickel oxalate crystal obtained as a result of subtraction of non spin polarized density from spin polarized one $[\rho_{sp}(r) - \rho_{nsp}(r)]$ (oxalate anion and NiO_6 octahedron environments are presented here only). *Yellow* (*darker*) and *blue* (*lighter*) regions correspond to positive and negative values, respectively (*in color*, *on-line*)

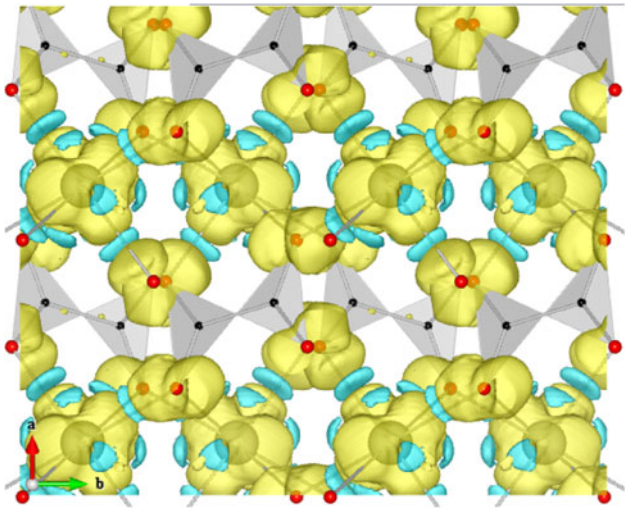

Fig. 9 Differential map of spin density obtained for anhydrous nickel oxalate $\rho^{\uparrow}(r) - \rho^{\downarrow}(r)$. *Yellow* (*darker*) and *blue* (*lighter*) regions correspond to positive and negative values, respectively (*in color*, *on-line*)

structure related to the necessity of preserving of such distances from oxygen atoms, to get the best overlap (maximum overlap integrals) of respective nickel and oxygen orbitals.

BVM calculations

Bond valences

The results of the calculations carried out according to Brown's bond valence model for anhydrous nickel oxalate are presented in Table 5 (atom and bond valences, deviations from theoretical valence and residual strain factors—local and global structure deviation from ideal one) and Table 6 (bond valences and bond lengths—theoretical and calculated from experimental data and resulting bond strains). The following set of equations fulfilling the valence sum rule for ideal structure were defined for anhydrous nickel oxalate (following the number and type of bonds determined in topological analysis of electron density):

$$\mathbf{Ni} = \mathbf{2r_1} + \mathbf{2r_2} + \mathbf{2r_3} = \mathbf{2} \cdot {}^1\!/_3 + \mathbf{2} \cdot {}^1\!/_3 + \mathbf{2} \cdot {}^1\!/_3 = \mathbf{2}$$

$$\mathbf{O_1} = \mathbf{r_1} + \mathbf{r_2} + \mathbf{r_4} = {}^1\!/_3 + {}^1\!/_3 + \mathbf{1} \cdot {}^1\!/_3 = \mathbf{2}$$

$$\mathbf{O_2} = \mathbf{r_3} + \mathbf{r_5} = {}^1\!/_3 + \mathbf{1} \cdot {}^2\!/_3 = \mathbf{2}$$

$$\mathbf{C} = \mathbf{r_4} + \mathbf{r_5} + \mathbf{r_6} = \mathbf{1} \cdot {}^1\!/_3 + \mathbf{1}{}^2\!/_3 + \mathbf{1} = \mathbf{4}$$

Table 5 Bond and atomic valences (s_{ij} and V_{ij}, respectively) with residual strain factors d_i and D, calculated from bond valence model for anhydrous nickel oxalate

Bond length/valence					V_{ij}	d_i	D
Ni		O_2	O_1	O_1			0.718
	R_{ij}	2.301	2.323	2.608			
	s_{ij}	0.174	0.164	0.076	0.828	1.172	
O_1		C	Ni	Ni			
	R_{ij}	1.257	2.323	2.608			
	s_{ij}	1.432	0.164	0.076	1.672	0.328	
O_2		C	Ni				
	R_{ij}	1.371	2.301				
	s_{ij}	1.053	0.174		1.227	0.773	
C		O_1	O_2	C			
	R_{ij}	1.257	1.371	1.590			
	s_{ij}	1.432	1.053	0.874	3.359	0.641	

From the results presented in Table 5 it follows that the crystal structure of anhydrous nickel oxalate is distinguished by large deviation from ideal structure predicted within BVM model (global instability index D equal to about 0.72 of valence units). Local instability indices d_i are positive for all atoms in the structure which means that on the average all bonds in this structure are too long (entire structure is loosely packed), which—taking into account the optimal bond lengths according to electron density overlapping in bond regions—results in this highly strained structure. Most strained within this structure are surroundings of nickel atoms (about +1.17 valence unit, v.u.; bonds too long, much too large octahedron with respect to

Table 6 Theoretical and experimental (from crystal structure data) bond valences s_{ij} and bond lengths R, relative bond length deviation from ideal one $\Delta R/R$ and bonds strain factors δ calculated for anhydrous nickel oxalate

NiC_2O_4	S_{ij}^{exp}	S_{ij}^{theor}	R_{theor}/Å	R_{exp}/Å	$\Delta R/R$/%	δ			
r_1 (Ni–O_1)	0.164	1/3	2.060	2.323	−11.29	δ_{Ni-O}	0.200	δ_{Ni-O1}	0.218
r_2 (Ni–O_1)	0.076	1/3	2.060	2.608	−20.99			δ_{Ni-O2}	0.159
r_3 (Ni–O_2)	0.174	1/3	2.060	2.301	−10.45			δ_{Ni-O3}	
r_4 (C–O_1)	1.432	1 1/3	1.284	1.257	2.11	δ_{C-O}	0.440	δ_{C-O1}	0.099
r_5 (C–O_2)	1.053	1 2/3	1.201	1.371	−12.40			δ_{C-O2}	0.614
r_6 (C–C)	0.874	1	1.540	1.590	−3.13	δ_{C-C}	0.126		
						δ_{Struct}	0.295		

ideal one). The surroundings of carbon and oxygen atom O_1 are quite similar and largely strained (about +0.64 and +0.77 v.u., respectively), and the least strained (but still quite significantly—about +0.32 v.u.) is the environment of O_1 oxygen atom.

Bond strains

The detailed analysis of strains present in the structure provides us with the additional information about bonding properties in this structure (Table 6): all three bonds formed by nickel with oxygen atoms are definitely too long (∼10–20 %), which means that they are under tensile stress. Taking into account the values of bond orders calculated from topological properties (Table 3) it becomes apparent when these bonds breaking is followed by release of significant amount of energy and structure reconfiguration. Carbon atom forms two bonds with oxygen atoms—first one slightly too short, with small compressive stress and the second one significantly too long, under the influence of tensile stress. O_1 oxygen atom forms two definitely too long bonds with nickel and one slightly too short with carbon (one can thus infer that in the proximity of this atom there should be distinct tendency to promote Ni–O bonds breaking during thermal decomposition process. Second oxygen atom O_2 forms only two bonds, both too long (∼10 %) one with nickel and one with carbon.

Conclusions

From the results of theoretical analysis of electronic structure and bonding properties in anhydrous nickel oxalate presented in this work, the following picture emerges: from the point of view of the geometry of the system due to the electrostatic interactions, the entire structure seems to be definitely too loose, thus the tensile stresses dominate in the crystal structure, which should result in strong structure readjustment, due to the breaking of subsequent bonds during thermal decomposition process. Chemical bonds in anhydrous nickel oxalate are distinguished by typical for anhydrous d-electron metal oxalates properties—Ni–O bonds have ionic-covalent character with dominating ionic component, while C–O and C–C bonds are typical shared interaction bonds. On a basis of the results obtained for total spin density and bond valence analysis we can propose the following pathway of thermal decomposition process as the most probable one: as a first one the weakest bond in this structure, namely C–C bond (r_6) should break. Due to large stresses in the structure (mostly tensile), one can expect almost instantaneous charge flow to C–O bonds and too much smaller extent to Ni–O bonds and shortening and strengthening of all remaining bonds (except r_4 which should become slightly longer and weaker). Carbon–oxide bond (r_4) is the strongest one in the structure and it will stay that way, even after it will weaken a little bit during the structure readjustment and stress relaxation process after C–C bond breaking, while r_5 bond will strengthen to comparable or even bigger extent than Ni–O bonds. Therefore, one can expect that nickel-oxygen bonds (r_1–r_3) should remain weaker than r_5 bond and in the following steps these bonds should break (the breaking of r_2 bond results in additional strengthening of r_5 bond, since O_2 atom will be bonded in this case only with carbon atom and thus this bond, due to the relaxation of tensile stress it will immediately become shorter and stronger). As a result, the most probable, suggested by theoretical analysis, sequence of bond breaking in anhydrous nickel oxalate during the process of thermal decomposition is as follows: as the first one, r_6 bond will be broken, then r_2 and subsequently r_1 and r_3 and the final products of such process will be metallic nickel and carbon dioxide—in agreement with the results of experiments [10, 38–42].

Acknowledgements This work was supported by Polish Ministry of Science and Higher Education under the project No. 2659/B/T02/2011/40.

References

1. Kondrashev YD, Bogdanov VS, Golubev SN, Pron GF. Кристаллическая структура упорядоченной фазы оксалата цинка й строение безводных оксалатов Fe^{2+}, Co^{2+}, Ni^{2+}, Cu^{2+} й Zn^{2+}. Zh Struct Khim. 1985;26:90–3.
2. Jeanneau E, Audebrand N, Louer D. β-CdC_2O_4. Acta Crystallogr. 2001;C57:1012–3.
3. Nopsiri Ch, Rangson M, Surasak N, Banjong B, Panpailin S, Naratip V. Non-isothermal kinetics of the thermal decomposition of sodium oxalate $Na_2C_2O_4$. J Therm Anal Calorim. 2012; 107(2):1023–9.
4. Brown ME, Dollimore D, Galwey AK. Comprehensive chemical kinetics. In: Bamford CH, Tipper CFH, editors. Reactions in solid state. Amsterdam: Elsevier; 1980.
5. Boldyrev VV, Nevyantsev IS, Mikhailov YI, Khayretdinov EF. K voprosu o myekhanizmye tyermichyeskogo razlozhyeniya oksalatov. Kinet Katal. 1970;11:367–73.
6. Borchardt HJ, Daniels F. The application of differential thermal analysis to the study of reaction kinetics. J Am Chem Soc. 1957;79:41–6.
7. Dollimore D. The thermal decomposition of oxalates. A review. Thermochim Acta. 1987;117:331–63.
8. Galwey AK. Theory of solid-state thermal decomposition reactions. J Therm Anal Calorim. 2012;109(3):1625–35.
9. Galwey AK, Brown ME. An appreciation of the chemical approach of V. V. Boldyrev to the study of the decomposition of solids. J Therm Anal Calorim. 2007;90(1):9–22.
10. Małecka B, Małecki A, Drożdż-Cieśla E, Tortet L, Llewellyn P, Rouquerol F. Some aspects of thermal decomposition of $NiC_2O_4{\cdot}2H_2O$. Thermochim Acta. 2007;466:57–62.
11. Dumitru R, Carp O, Budrugeac P, Niculescu M, Segal E. Non-isothermal decomposition kinetics of $[CoC_2O_4{\cdot}2.5H_2O]_n$. J Therm Anal Calorim. 2011;103(2):591–6.
12. Koleżyński A, Małecki A. Theoretical studies of thermal decomposition of anhydrous cadmium and silver oxalates. Part I. Electronic structure calculations. J Therm Anal Calorim. 2009; 96(1):161–5.
13. Koleżyński A, Małecki A. Theoretical studies of thermal decomposition of anhydrous cadmium and silver oxalates. Part II. Correlations between the electronic structure and the ways of thermal decomposition. J Therm Anal Calorim. 2009;96(1):167–73.
14. Koleżyński A, Małecki A. First principles studies of thermal decomposition of anhydrous zinc oxalate. J Therm Anal Calorim. 2009;96(2):645–51.
15. Koleżyński A, Małecki A. Theoretical approach to thermal decomposition process of chosen anhydrous oxalates. J Therm Anal Calorim. 2009;97(1):77–83.
16. Koleżyński A, Małecki A. Theoretical analysis of electronic structure and structural properties of anhydrous calcium oxalate. J Therm Anal Calorim. 2009;99(2):947–55.
17. Koleżyński A, Małecki A. Theoretical analysis of electronic and structural properties of anhydrous mercury oxalate. J Therm Anal Calorim. 2010;101(2):499–504.
18. Koleżyński A, Thermal decomposition of anhydrous metal oxalates—theoretical analysis (habilitation monograph—in polish). Ceramika/Ceramics. 2010;109.
19. Blaha P, Schwarz K, Madsen GKH, Kvasnicka D, Luitz J, Schwarz K. WIEN2k, An augmented plane wave + local orbitals program for calculating crystal properties. Wien: Techn. Universität Wien; 2001. ISBN 3-9501031-1-2.
20. Slater JC. Wave functions in a periodic potential. Phys Rev. 1937;51(10):846–51.
21. Loucks TL. Augmented plane wave method. NewYork: Benjamin; 1967.
22. Andersen OK. Simple approach to the band-structure problem. Solid State Commun. 1973;13(2):133–6.
23. Hamann DR. Semiconductor charge densities with hard-core and soft-core pseudopotentials. Phys Rev Lett. 1979;42(10):662–5.
24. Wimmer E, Krakauer H, Weinert M, Freeman AJ. Full-potential self-consistent linearized-augmented-plane-wave method for calculating the electronic structure of molecules and surfaces: O2 molecule. Phys Rev B. 1981;24(2):864–75.
25. Singh DJ. Planewaves, pseudopotentials and the LAPW method. Dordrecht: Kluwer Academic Publishers; 1994.
26. Perdew JP, Burke K, Ernzerhof M. Generalized gradient approximation made simple. Phys Rev Lett. 1996;77(18): 3865–8.
27. Aroyo MI, Perez-Mato JM, Orobengoa D, Tasci E, de la Flor G, Kirov A. Crystallography online: bilbao crystallographic server. Bulg Chem Commun. 2011;43(2):183–97.
28. Aroyo MI, Perez-Mato JM, Capillas C, Kroumova E, Ivantchev S, Madariaga G, Kirov A, Wondratschek H. Bilbao crystallographic server I: Databases and crystallographic computing programs. Z Krist. 2006;221(1):15–27.
29. Aroyo MI, Kirov A, Capillas C, Perez-Mato JM, iWondratschek H. Bilbao crystallographic server. II. Representations of crystallographic point groups and space groups. Acta Crystallogr A. 2006;A62:115–28.
30. Bader RFW. Atoms in molecules: a quantum theory. Oxford: Clarendon Press; 1990.
31. Pauling L. The nature of the chemical bond. New York: Cornell University Press; 1960.
32. Bader RFW, Slee TS, Cremer D, Kraka E. Description of conjugation and hyperconjugation in terms of electron distributions. J Am Chem Soc. 1983;105(15):5061–8.
33. Cioslowski J, Mixon ST. Covalent bond orders in the topological theory of atoms in molecules. J Am Chem Soc. 1991;113(11):4142–5.
34. Howard ST, Lamarche O. Description of covalent bond orders using the charge density topology. J Phys Org Chem. 2003; 16(2):133–41.
35. Brown ID. The chemical bond in inorganic chemistry. The bond valence model. Oxford: Oxford University Press; 2002.
36. Koleżyński A. FP-LAPW study of anhydrous cadmium and silver oxalates: electronic structure and electron density topology. Phys B. 2010;405:3650–7.
37. Otero-de-la-Roza A, Blanco MA, Pendás AM, Luaña V. Critic: a new program for the topological analysis of solid-state electron densities. Comput Phys Commun. 2009;180:157–66.
38. Nikumbh AK, Athare AE, Raut BV. A study of the thermal decomposition of cobalt(II) and nickel(II) oxalate dihydrate using direct current electrical conductivity measurements. Thermochim Acta. 1991;186:217–33.
39. Coetzee A, Eve DJ, Brown ME. Thermal analysis of some mixed metal oxalates. J Therm Anal Calorim. 1993;39:947–73.
40. El-Wahab MMMA, Mahfouz RM. Gamma irradiation effects on the electrical conductivity behaviour and thermal decomposition induction period in nickel oxalate. Thermochim Acta. 1996; 274:281–7.
41. Majumdar R, Sakar P, Ray P, Mukhopadhyay MR. Secondary catalytic reactions during thermal decomposition of oxalates of zinc, nickel and iron(II). Thermochim Acta. 1999;335:43–53.
42. Zhan D, Conga C, Diakite K, Tao Y, Zhang K. Kinetics of thermal decomposition of nickel oxalate dihydrate in air. Thermochim Acta. 2005;430:101–5.